Preprints of the 21st IFAC World Congress (Virtual)
Berlin, Germany, July 12-17, 2020

Hysteresis in nanopositioning systems driven by dual-stack differential driving piezoelectric actuators ⋆

Massoud Hemmasian Ettefagh * **Ali Bazaei** ** **Zhiyue Wang** *
Zhiyong Chen ** **Hai-Tao Zhang** * **Stephane Regnier** ***
Mokrane Boudaoud ***

* *School of Artificial Intelligence and Automation, Huazhong University of Science and Technology, Wuhan, China, (e-mail: massoud.ettefagh@gmail.com; wzy1998@hust.edu.cn ; zht@mail.hust.edu.cn).*
** *School of Electrical Engineering and Computing, University of Newcastle Australia, Callaghan, NSW Australia (e-mail: {ali.bazaei; zhiyong.chen} @newcastle.edu.au*
*** *Institut des Systèmes Intelligents et de Robotique, Sorbonne Université, Paris, France, (e-mail: {stephane.regnier; mokrane.boudaoud}@sorbonne-universite.fr)*

Abstract: The existence of hysteresis phenomenon in piezoelectric actuators of nanopositioners adversely affects their performance, e.g. image distortion in Atomic Force Microscopy. A usual approach to circumnavigate hysteresis nonlinearity is feedforward compensation where the performance depends extensively on the accuracy of the hysteresis model. To achieve accurate modeling of hysteresis in nanopositioners driven by piezoelectric stacks, we used a dual-stack differential driving configuration. Comparing hysteresis in single-stack piezoelectric actuators with dual-stack piezoelectric actuators in differential driving configuration, we observed a more symmetric behavior for the hysteresis in dual-stack differential driving actuators. Then, we modeled the differential driving configuration by utilizing coupled electromechanical equations with hysteresis models applied to them. In particular, Duhem and Prandtl-Ishlinskii (P–I) methods were used for hysteresis modeling. Based on the models and experimental data, we observed that the maximum value of the Duhem modeling error reduced from 9.63% for the nondifferential configuration to 1.85% for the differential configuration. For the P–I method, the maximum modeling error decreased from 7.46% to 2.77%. This observation shows that the dual-actuated differential driving configuration improves hysteresis modeling accuracy. Therefore, this configuration is a suitable choice for the applications where accuracy is of prime importance.

Keywords: piezoelectric, hysteresis, modeling, dual-stack, differential-drive

1. INTRODUCTION

Thanks to their ability to generate large forces as well as their high resolution, fast response, high stiffness, and small size, Piezoelectric Actuators (PAs) are widely utilized in applications that involve micro- and nano-scale positioning. However, PAs suffer from the highly nonlinear behavior between the inputs and the outputs. Hysteresis and creep are two nonlinear phenomena that, if not compensated for, can severely deteriorate the performance (Cao and Chen, 2015). Creep effect is limited to slow operating speeds at low frequencies, and its effect diminishes as the applied frequency increases. Hysteresis effect, on the other hand, is significant in all frequencies, and its value becomes notable when the PA displacement surpasses 10% of the full range displacement (Ru et al., 2016). Hysteresis is known as the main nonlinear effect of PAs as it causes tracking errors up to 20% of the full-range displacement (Cao and Chen, 2015). The positioning error caused by hysteresis, for example, can cause image distortion in Atomic Force Microscopes (AFMs) driven by PAs. Therefore, accurate modeling and precise control of hysteresis are of prime importance in applications where long-range displacement with high resolution is required.

Generally, there are four methods to deal with hysteresis distortion in a PA: 1- small signal actuation, 2- charge control, 3- feedback control, and 4- feedforward control. In order to keep the behavior of a PA linear, the low voltage actuation method restricts the PA's displacement to $5-10\%$ of the full-range motion (Ru et al., 2016). Several studies have shown that driving PAs with charge, or current rather than voltage substantially decrease hysteresis distortion (Devasia et al., 2007). Feedback control

⋆ This work has been supported by the National Natural Science Foundation of China under grant Number 51729501, and the Project PolyREM (Emergence Sorbonne Université), the French government research program Investissements d'avenir through the Robotex Equipment of Excellence (ANR-10-EQPX-44).

techniques are regarded as the primary method to cancel positioning errors and reject effect of disturbances when the actuation input is voltage. Cancellation of nonlinear effects and precise positioning in feedback control methods are achievable at the cost of using high feedback gains, which produces its own problems such as excessive projected noise (Bazaei et al., 2015). Nonlinear effects have also been dealt with by feedback control using a specific internal model design in the framework of output regulation theory (Chen et al., 2017). Because of lightly damped resonant modes in piezo-driven nanopositioners, they have low gain margins and large feedback gains tend to make the system unstable, which results in a compromise between stability and performance (Devasia et al., 2007). Furthermore, as the hysteresis phenomenon in PAs exhibits nonlocal memory, the displacement of PAs depends on the history of the inputs as well as the current input. Hence, several displacement values can be obtained from the same input voltage, which adds more difficulties to the feedback control system (Devasia et al., 2007). Feedforward controllers are employed to help the feedback control law and improve the system's performance without weakening stability. The primary purpose of a feedforward controller system is to cancel known disturbances and compensate for hysteresis and creep distortions. Since the hysteresis is the main source of nonlinear behavior of PAs, several studies have been carried out to compensate it, see Cao and Chen (2015); Devasia et al. (2007) and references therein for more details.

Many feedforward controllers use a model of hysteresis to compensate for its adverse effect (Eielsen et al., 2012). Therefore, the performance of these controllers relies thoroughly on the accuracy of the model they used. On this basis, several models have been introduced to describe hysteresis. To name a few, Preisach, Prandtl-Ishlinskii (P–I), Duhem, and Bouc-Wen are some popular methods for hysteresis modeling in control systems for piezo-driven nanopositioners. A more detailed list is available in survey papers such as Cao and Chen (2015); Devasia et al. (2007).

Piezoelectric Stack Actuators (PSAs) are designed to tolerate large axial compresive loads and are able to generate large values of pushing force (see Fig. 1). This unidirectional nature to make displacement in only one direction can be a shortcoming. Furthermore, as PSAs are sensitive to environmental conditions (Fett and Thun, 1998), their conventional unidirectional applications, shown in Fig. 1, make the system susceptible to environmental changes, e.g., temperature. Therefore, this asymmetric configuration could deteriorate the system's performance, especially in highly accurate positioning devices such as nanopositioners or AFMs. To address these limitations, dual-stack differential driving systems ,Fig. 1 (right), were addressed in a number of publications (Schitter et al., 2007; Bazaei et al., 2019b).

The main contribution of this paper is to study the hysteresis effect in dual-stack differentially piezo-driven nanopositioning systems. First, we introduce differential equations to describe hysteresis in the differential drive configuration. Then, we observe from experimental data that the hysteresis distortion in the differential driving configuration is more symmetric than the unidirectional configuration. Next, we employ Duhem and Prandtl-Ishlinskii (P–I) models to capture hysteresis behavior, and showed that the differential driving configuration improves modeling error.

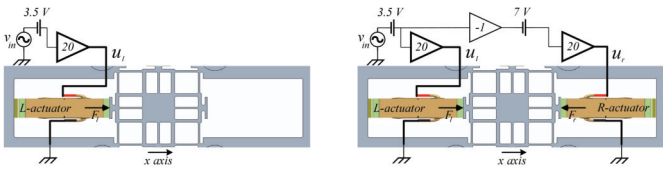

Fig. 1. Unidirectional actuation (left) and dual actuated differential driving actuation (right) methods.

The rest of this paper is organized as follows. In section 2, we introduce differential drive configuration of PSAs for a nanopositioner and the Duhem and P–I models for hysteresis in PSAs. Experimental setup, method of obtaining data, and early observations are represented in section 3. Section 4 is devoted to studying hysteresis in nanopositioners driven by dual-stack differential driving PSAs. Finally, the conclusions are drawn in section 5.

2. MODELING

The constitutive equation of piezoelectric materials (IEEE, 1988) for a multi-layer PSA results in

$$F = Tv - K_I x, \tag{1}$$
$$Q = Tx + Cv, \tag{2}$$

where K_I, T, and C are defined constants, F $[N]$ is the force applied by the PSA, Q $[Cb]$ is the total charge of the stack, x $[m]$ is the longitudinal displacement of the stacks, and v $[V]$ is the applied voltage to the PSA.

Using (1)–(2), a schematic drawing of a nanopositioning system driven by a pair of identical PSA in the differential driving configuration is shown in Fig. 2. Using mass-spring-damper system, the figure illustrates the interaction between electrical and mechanical parts for the $x-$axis of motion. By using this approximate model, we consider the first mode shape of the stage for the case in which the excitation frequency is well below the fundamental frequency. A similar situation is valid for the $y-$axis of motion.

In Fig. 2, M_p denotes the inertia term (effective mass) for the PSA in the first eigenmode of the longitudinal vibration (Stokey, 1988), M_s and K_s denote inertia and stiffness terms, respectively, for the stage in the $x-$axis of motion, and K_0 represents the stiffness of the stack-stage interaction port. The force applied to the point-mass model of the PSAs is obtained from (1). Following Goldfarb and Celanovic (1997), the hysteresis nonlinearity $\mathbf{H}$ is serially connected to the electrical part of the PSA; therefore, the applied voltage at the electromechanical port is $v_{(\cdot)} = u_{(\cdot)} - v^h_{(\cdot)}$, where $v^h_{(\cdot)}$ is the disturbance voltage due to the hysteresis effect, $u_{(\cdot)}$ is the total voltage applied to the PSA, and $(\cdot)$ can be either (l) or (r), representing left or right actuator, respectively.

The main difference of our model with the conventional models used for PSA based positioning systems, see e.g. Adriaens et al. (2000), is the introduction of K_0 between piezo body and the stage in the middle. This stiffness is necessary to comply with the conservation of energy at the

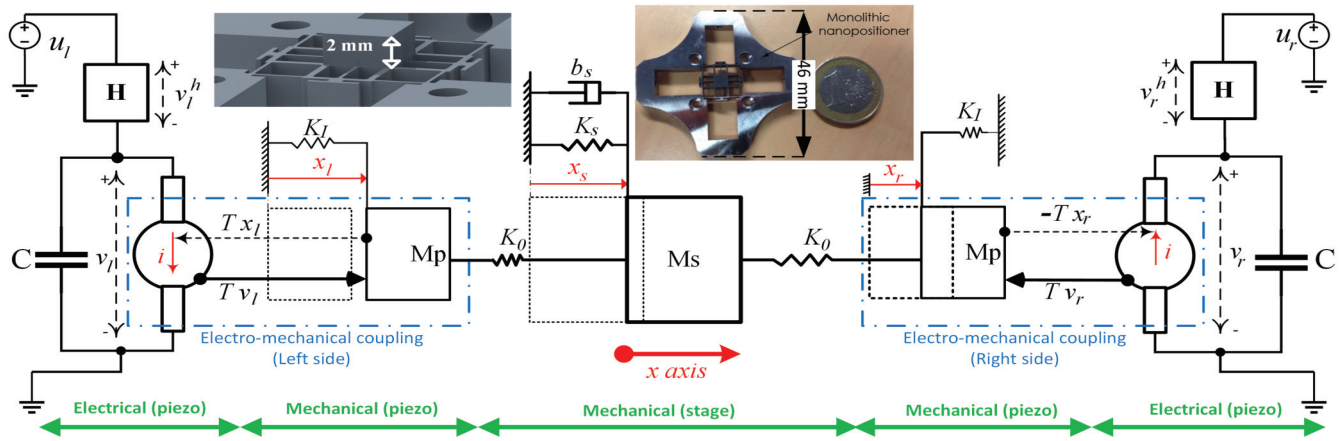

Fig. 2. Dual actuated nanopositioning stage and its simplified electro-mechanical model. Solid-line and dashed-line show the model after and before actuation, respectively

port of interaction when the PSAs are electrically biased. In this respect, when a DC voltage is applied identically to the left and right PSAs, $u_l = u_r = \overline{u}$, the flexibility between M_s and M_ps causes the left and right PSAs to displace $\frac{T(\overline{u}-v^h)}{(K_I+K_0)}$ and $-\frac{T(\overline{u}-v^h)}{(K_I+K_0)}$, respectively, while the displacement of the stage is still zero.

Employing (1), (2), and Fig. 2, the set of governing electromechanical equations is presented below. In (7), x_r applies a compressive force to the right PSA, therefore, its effect appears with negative sign.

$$M_p\ddot{x}_l + (K_I + K_0)x_l - K_0x_s = T(u_l - v_l^h), \quad (3)$$
$$M_s\ddot{x}_s + +b_s\dot{x}_s - K_0x_l + (K_s + 2K_0)x_s - K_0x_r = 0, \quad (4)$$
$$M_p\ddot{x}_r + (K_I + K_0)x_r - K_0x_s = -T(u_r - v_r^h), \quad (5)$$
$$Q_l = C(u_l - v_l^h) + Tx_l, \quad (6)$$
$$Q_r = C(u_r - v_r^h) - Tx_r. \quad (7)$$

2.1 Hysteresis models

The Duhem model is a first-order differential equation that is originally developed to explain rate-independent magnetic hysteresis behavior in ferromagnetic materials (Adriaens et al., 2000). The equation, then, proves its validity to model hysteresis behavior in piezoelectric materials through several studies, e.g., Adriaens et al. (2000); Lin and Lin (2012). The first-order differential form, with three parameters to be identified, has made Duhem method attractive to design model-based control systems with hysteresis compensation. The model for the hysteresis effect between input $x(t)$ and output (hysteresis value) $y(t)$ is given by

$$\dot{y}(t) = \alpha|\dot{x}(t)|\left[\beta x(t) - y(t)\right] + \gamma\dot{x}(t) \quad (8)$$

where $\alpha, \beta, \gamma > 0$ are model's parameters that are to be identified.

The P–I model characterize the hysteresis behavior between input $x(t)$ and output $y(t)$ by a finite series of *play and stop* operators. Assuming the input $x(t), t_i \le t \le t_{i+1}$, $i = 1, \cdots, N$ belongs to the space of piecewise monotone continuous functions, the play operator is defined as

$$\mathcal{P}_r[x](0) = p_r(x(0), x) = 0 \quad (9)$$
$$\mathcal{P}_r[x](t) = p_r(x(t), \mathcal{P}_r[x](t_i)), \quad t_i \le t \le t_{i+1} \quad (10)$$
$$p_r(x(t), \mathcal{P}_r[x](t_i)) = \max\left(x(t) - r, \min\left(x(t) + r, \mathcal{P}_r[x](t_i)\right)\right) \quad (11)$$

where r is the input threshold. The output $y(t)$ of the P–I model is defined as (Gu et al., 2013)

$$y(t) = a_0x(t) + \int_0^\infty a(r)\mathcal{P}_r[x](t)\ \mathrm{d}r \quad (12)$$

where $a(r)$ is the density function that controls the size and shape of the hysteresis curve. This function converges to zero as $r \to \infty$; therefore, in practice, the upper limit of the integral is truncated to a limited large number. In (12), coefficient a_0 and function $a(r)$ are the parameters that must be identified.

In the literature of control systems for hysteresis compensation in PAs, there are two methods to incorporate a hysteresis model into the electromechanical equations (3)–(7). The first method considers voltage across the hysteresis box (see Fig. 2) and the total charge of the piezoelectric as the input and output of the hysteresis model, respectively. The second method, however, considers the driving voltage and the stage displacement as the input and output, respectively. Because the hysteresis models used for control design purposes are phenomenological base, both methods are acceptable provided that they produce accurate models. Examples of the first method include Adriaens et al. (2000); Lin and Lin (2012), and examples of the second method are given in Fleming and Leang (2014); Rakotondrabe (2010); Habineza et al. (2015). In this study, we used the second method with the procedure explained in section 4.

3. EXPERIMENTS AND EARLY OBSERVATION

Shown in Fig. 2, a custom-made symmetrical flexure-based nanopositioning stage is used in this study (Bazaei et al., 2019a). The symmetrical structure of the monolithic stage accommodates for single and dual PSA for unidirectional and differential driving configurations, respectively, as shown in Fig. 1. The middle square stage displaces along x and/or y axes by PSAs (Thorlabs PK4DLP2) either in unidirectional (1) or differential driving configuration.

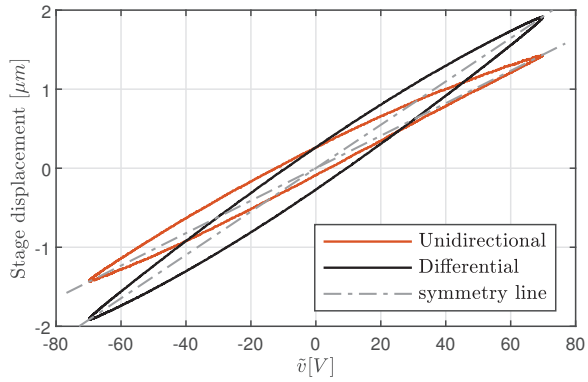

Fig. 3. Hysteresis curves of the stage displacement for unidirectional and differential driving configurations.

The PSAs are installed and preloaded in their places by preload screws (not shown in the figure). The displacement of the stage is measured by a LASER interferometer sensor (SIOS SM-05), which uses the extruded middle stage as the reflecting surface. A dSPACE board is used to generate input signals and collect sensor data.

A dual-channel voltage amplifier (FLC Electronics A400DI) amplifies the input signal and small bias voltages before being applied to the actuators at the left and right sides (L– and R–actuators). The amplifier has an in-built phase inverter that shifts 180° its input phase. In order to measure the hysteresis curve accurately, the excitation frequency must be chosen so that neither the creep nor the dynamic (phase lag) behaviors influence the curve (Rakotondrabe et al., 2009). The fundamental frequency of the nanopositioning stage and PSAs are 17 and 250 $[kHz]$, respectively (Bazaei et al., 2019b); therefore, we selected $\omega = 750$ $[Hz]$ as the operating frequency in which the experimental data are collected. Shown schematically in Fig. 1, the L-actuator in the unidirectional configuration is driven by $u_l = 70+70\sin(2\pi\omega t)$ $[V]$. For the configuration of differential driving actuation, the driven voltage for the L– and R–actuators are $u_l = 70 + 70\sin(2\pi\omega t)$ $[V]$ and $u_r = 70 - 70\sin(2\pi\omega t)$ $[V]$, respectively.

During the experiment, the input voltage $u_l(t)$ and the stage displacement were collected and imported to Matlab for identification and modeling. Then, we plotted the hysteresis curves for the unidirectional and differential driving configuration in Fig. 3. In the figure, the stage displacement is drawn against the alternative voltage part $\tilde{v}$ of the L–actuator. It can be seen in the figure that the hysteresis curve of the differential driving configuration is more symmetric than that of the unidirectional configuration. To show this symmetric behavior more clear, we drew the symmetry line of each curve in the figure.

It is shown in Ru et al. (2016) that the hysteresis effect in PSAs is negligible if they are actuated within their 10% of the full-range displacement. Therefore, in order to determine the linear part of the systems' dynamics, we actuated the PSAs with a small-signal voltage across a wide frequency range. The result is given in the bode diagrams of Fig. 4 for unidirectional and differential driving configurations. Since the interested working bandwidth of the system is well below its first natural frequency,

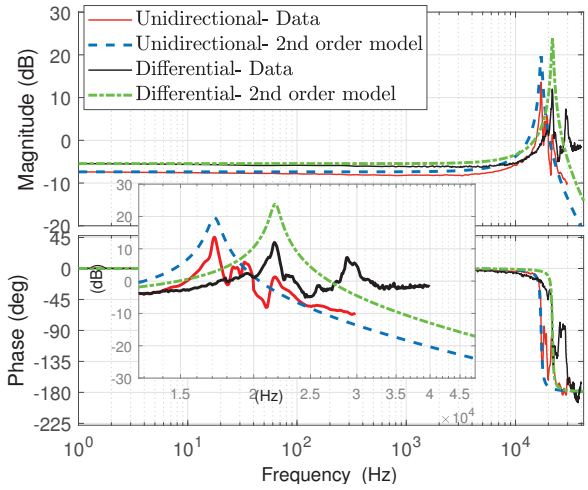

Fig. 4. The frequency response of the nanopositioning stage under small-signal actuation.

we identified each configuration by fitting a second order transfer function on it and disregarding the higher frequency contents. The identified transfer function for each configuration is expressed as

$$G(s) = \frac{a_0}{1 + 2\zeta(\frac{s}{\omega_n}) + (\frac{s}{\omega_n})^2} \tag{13}$$

where $(a_0,\ \zeta, \omega_n)$ is $(0.43, 0.022, 1.08e5)$ for unidirectional and $(0.534, 0.017, 1.37e5)$ for differential configurations. A short comparison between frequency responses of the unidirectional and differential drive configurations shows that the latter improves the natural frequency and the dc gain. The reason is explained in the next section.

4. HYSTERESIS IN DUAL-STACK DIFFERENTIAL-DRIVE ACTUATORS

In this section, we explain the comparative study performed to highlight the improvement in hysteresis behavior of the dual-stack differential drive actuator. First, we describe individual integration of Duhem (8) and P–I (12) models to the electromechanical system (3)–(7) to capture hysteresis behavior. Next, the identification procedure is explained. Then, we compare and analyze the hysteresis models in the nanopositioner actuated with dual-stack differential drive configuration and the one actuated with a single-single stack unidirectional configuration.

By assuming $K_0 \to \infty$, we simplify (3)–(5) to a single equation to utilize the Duhem model between input voltage and stage displacement. Note that this assumption is only valid after that the PSAs are electrically biased and find their new equilibrium points. Assuming $K_0 \to \infty$ in the unidirectional configuration results in the following set of electromechanical equations with Duhem model for hysteresis (Fleming and Leang, 2014).

$$(M_s + M_p)\ddot{x}_s + b_s\dot{x}_s + (K_I + K_s)x_s = T(u_l - v_l^h), \tag{14}$$
$$\dot{x}_s = \alpha|\dot{u}_l|\,[\beta u_l - x_s] + \gamma\dot{u}_l, \tag{15}$$
$$u_l = 70 + 70\sin(2\pi\omega t). \tag{16}$$

With a similar assumption in the differential driving configuration, the following equations are obtained

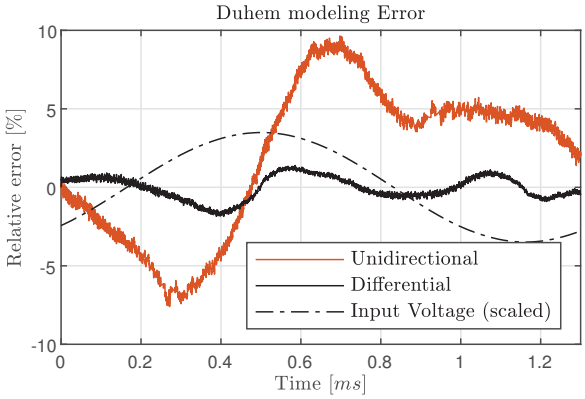

Fig. 5. Relative error of Duhem modeling in one cycle for unidirectional and differential driving configurations.

$$(M_s + 2M_p)\ddot{x}_x + b_s\dot{x}_s + (2K_I + K_s)x_s = T(u_l - u_r) - T(v_l^h - v_r^h), \quad (17)$$

$$\dot{x}_s = \alpha|\dot{u}_l|\,[\beta u_l - x_s] + \gamma\dot{u}_l, \quad (18)$$

$$u_l = 70 + 70\sin(2\pi\omega t), \quad (19)$$

$$u_r = 70 - 70\sin(2\pi\omega t). \quad (20)$$

For the P–I modeling of hysteresis, (15) and (18) are substituted with

$$x_s(t) = a_0 u_l(t) + \sum_{i=1}^{N} f_i \mathcal{P}_i[u_l](t) \quad (21)$$

where N denotes the number of adopted play operators, and f_i is the weighted coefficient for the threshold r_i. Using (21), the identification problem casts down to identifying $N+1$ parameters $a_0, f_1, \cdots, f_N$. The relation between the weighted coefficients and density function is (Gu et al., 2013)

$$f_i = a(r_i)(r_i - r_{i-1}), \quad (22)$$

$$r_i = \frac{i-1}{N}\|u_l(t)\|_\infty. \quad (23)$$

It should be mentioned that in (17)–(21), the hysteresis models capture the overall hysteresis effect associated with $(v_l^h - v_r^h)$ rather than the effect of each term individually.

To identify hysteresis parameters in (15) and (18) we use least square method. Having known x_s and u_l from the experiments, we rewrite (18) as

$$y(\tau) - y(\tau_0) = \alpha\beta J_1(\tau) - \alpha J_2(\tau) + \gamma J_3(\tau) \quad (24)$$

in which $J_1(\tau) = \int_0^\tau u(t)|\dot{u}(t)|\,\mathrm{d}t$, $J_2(\tau) = \int_0^\tau x_s(t)|\dot{u}(t)|\,\mathrm{d}t$, and $J_3(\tau) = u(\tau) - u(0)$. Then, the unknown parameters $\Theta = [\alpha\beta, \ -\alpha, \ \gamma]^T$ are obtained from parameter identification with pseudo-inverse methods. The identified parameters for the unidirectional and differential driving configurations are given in Table 1. Based on the identified values, the Duhem model is constructed and compared to the experimental data for each configuration. The result of the comparison is presented in Fig. 5 for one period of the input u_l. According to the figure and the reported error values in Table 1, the Duhem modeling error for the differential driving configuration is significantly reduced.

A similar approach is used to identify parameters of the P–I model (21), i.e. considering u_l and x_s as input and output in P–I equation (12). The identified parameters

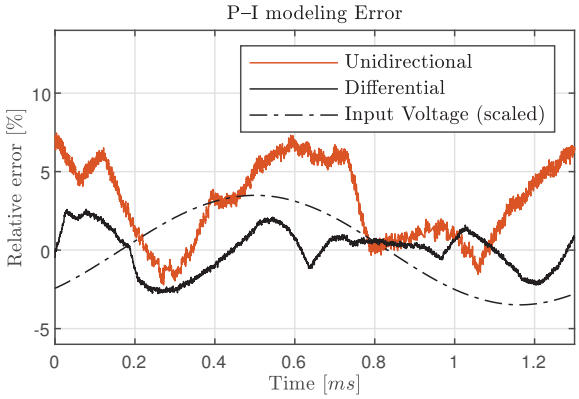

Fig. 6. Relative error of P–I modeling in one cycle for unidirectional and differential driving configurations.

Table 1. Identification summary of the Duhem model for Hysteresis.

Configuration	Identified parameters α	β	γ	Modeling error Maximum	RMS*
Unidirectional	0.0036	0.0696	0.0256	9.63%	5.09%
Differential	0.0095	0.0394	0.0256	1.85%	0.73%

*Root Mean Square

Table 2. Identification summary of the P–I model for Hysteresis.

Configuration	Identified parameters $[a_0,\ f_1,\ f_2,\ f_3,\ f_4]$ $[f_5,\ f_6,\ f_7,\ f_8,\ f_9]$	Modeling error Max.	RMS*
Unidirectional	$[11.5, 13.9, -1.3, 3.2, 0.9]\times10^{-3}$ $[3.2, -0.3, -1.1, 7.7, -10.6]\times10^{-3}$	7.46%	4.02%
Differential	$[14.9, 9.8, -1.3, 2.5, 1.2]\times10^{-3}$ $[1.2, 1.3, -0.1, 4.9, -3.9]\times10^{-3}$	2.77%	1.33%

*Root Mean Square

and modeling error for the unidirectional and differential driving configurations are given in Table 2 and Fig. 6. The results show that the maximum modeling error has decreased from 7.46% for the unidirectional configuration to 2.77% for the differential case. Similarly, the RMS error shows a consistent reduction. The number of identified parameters are selected in such a way that further increase in it does not improve the error.

The hysteresis distortion for each configuration is shown in Fig. 7. To do this, $K_I + K_s$ is determined from finite element analysis. Next, we use (13) and (14) to identify M_s, M_p and b_s. Finally, by substituting (16) in (14) and (15), we obtain the hysteresis distortion Tv_l^h. A similar approach is used to determine hysteresis distortion for differential drive configuration. According to this figure, the hysteresis distortion in the differential driving configuration is about 50% more than the unidirectional configuration. This increase can be attributed to the number of piezo stacks used in each configuration. While the unidirectional configuration employs one piezo stack, the differential drive configuration employs two piezo stacks; therefore, as the figure shows, an increase in the hysteresis distortion is expected in the differential drive configuration. Additionally, as the displacement range in the dif-

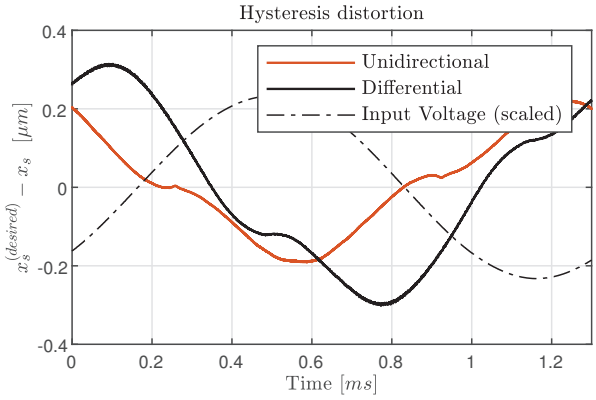

Fig. 7. Hysteresis distortion in stage displacement for the unidirectional and differential driving configurations. $K_I + K_s = 31.17$ $[N/\mu m]$, $M_p + M_s = 2.68$ $[gr]$, $b = 12.72$ $[N.s/m]$, and Duhem model is used to find the hysteresis distortion.

ferential drive configuration has increased in comparison with the one of the unidirectional case, a higher hysteresis distortion is expected. However, since this distortion is modeled more accurately and can be canceled via a feedforward controller, the increase in the value is not prohibiting.

5. CONCLUSION

We examine dynamics and hysteresis effect in nanopositioning systems driven by piezoelectric stack actuators in the differential driving configuration. An electromechanical model is presented to describe the configuration. Based on the experimental data and two distinctive models, the hysteresis effect in differential driving configuration is compared with the unidirectional configuration. As the differential driving configuration presents a more symmetric behavior in the hysteresis curve, it follows that the hysteresis modeling error for this configuration is considerably less than that of the unidirectional configuration. This reduction in modeling error is advantageous in the accuracy improvement of nanopositioning systems.

The differential drive configuration used in work requires a pair of piezoelectric actuators for each axis of movement, which could increase the overall size of the stage. The result of this study could be used in design and control of high-accurate nanopositioning stages.

REFERENCES

Adriaens, H., De Koning, W.L., and Banning, R. (2000). Modeling piezoelectric actuators. IEEE/ASME transactions on mechatronics, 5(4), 331–341.

Bazaei, A., Boudaoud, M., Hemmasian Ettefagh, M., Chen, Z., and Régnier, S. (2019a). Displacement sensing by piezoelectric transducers in high-speed lateral nanopositioning. IEEE Sensors Journal.

Bazaei, A., Boudaoud, M., Hemmasian Ettefagh, M., Chen, Z., and Régnier, S. (2019b). In-situ semiconductor position sensor for differentially piezo-driven nanopositioners. In 2019 IEEE SENSORS, 1–4. IEEE.

Bazaei, A., Maroufi, M., and Moheimani, S.R. (2015). Noise resilient 2-dof washout tracking controller for nanopositioning systems subject to sensor drift. In 2015 American Control Conference (ACC), 1199–1204. IEEE.

Cao, Y. and Chen, X. (2015). A survey of modeling and control issues for piezo-electric actuators. Journal of Dynamic Systems, Measurement, and Control, 137(1), 014001.

Chen, Z., Zheng, J., Zhang, H.T., and Ding, H. (2017). Tracking of piezoelectric actuators with hysteresis: A nonlinear robust output regulation approach. International Journal of Robust and Nonlinear Control, 27(15), 2610–2626.

Devasia, S., Eleftheriou, E., and Moheimani, S.R. (2007). A survey of control issues in nanopositioning. IEEE Transactions on Control Systems Technology, 15(5), 802–823.

Eielsen, A.A., Gravdahl, J.T., and Pettersen, K.Y. (2012). Adaptive feed-forward hysteresis compensation for piezoelectric actuators. Review of Scientific Instruments, 83(8), 085001.

Fett, T. and Thun, G. (1998). Determination of room-temperature tensile creep of pzt. Journal of Materials Science Letters, 17(22), 1929–1931.

Fleming, A.J. and Leang, K.K. (2014). Design, Modeling and Control of Nanopositioning Systems, chapter 11,12. Springer.

Goldfarb, M. and Celanovic, N. (1997). Modeling piezoelectric stack actuators for control of micromanipulation. IEEE Control Systems Magazine, 17(3), 69–79.

Gu, G.Y., Zhu, L.M., and Su, C.Y. (2013). Modeling and compensation of asymmetric hysteresis nonlinearity for piezoceramic actuators with a modified Prandtl–Ishlinskii model. IEEE Transactions on Industrial Electronics, 61(3), 1583–1595.

Habineza, D., Rakotondrabe, M., and Le Gorrec, Y. (2015). Bouc–Wen modeling and feedforward control of multivariable hysteresis in piezoelectric systems: Application to a 3-dof piezotube scanner. IEEE Transactions on Control Systems Technology, 23(5), 1797–1806.

IEEE (1988). IEEE standard on piezoelectricity. ANSI/IEEE Std 176-1987. doi: 10.1109/IEEESTD.1988.79638.

Lin, C.J. and Lin, P.T. (2012). Tracking control of a biaxial piezo-actuated positioning stage using generalized Duhem model. Computers & Mathematics with Applications, 64(5), 766–787.

Rakotondrabe, M. (2010). Bouc–Wen modeling and inverse multiplicative structure to compensate hysteresis nonlinearity in piezoelectric actuators. IEEE Transactions on Automation Science and Engineering, 8(2), 428–431.

Rakotondrabe, M., Clévy, C., and Lutz, P. (2009). Complete open loop control of hysteretic, creeped, and oscillating piezoelectric cantilevers. IEEE Transactions on Automation Science and Engineering, 7(3), 440–450.

Ru, C., Liu, X., Sun, Y., et al. (2016). Nanopositioning Technologies, chapter 7. Springer.

Schitter, G., Astrom, K.J., DeMartini, B.E., Thurner, P.J., Turner, K.L., and Hansma, P.K. (2007). Design and modeling of a high-speed afm-scanner. IEEE Transactions on Control Systems Technology, 15(5), 906–915.

Stokey, W.F. (1988). Vibration of systems having distributed mass and elasticity. Shock and vibration Handbook, 7.1–7.50.